

Lighting up dark plasmon modes in bowtie nanoantenna with electron beam

Kin Hung Fung^{1,2,#}, Anil Kumar^{3,#}, and Nicholas X. Fang^{1,*}

¹ Department of Mechanical Engineering, Massachusetts Institute of Technology,
Cambridge, Massachusetts 02139

² Department of Mechanical Science and Engineering,
University of Illinois at Urbana-Champaign, Urbana, Illinois 61801

³ Department of Electrical and Computer Engineering,
University of Illinois at Urbana-Champaign, Urbana, Illinois 61801

The authors contributed equally to this work.

* Corresponding author: nicfang@mit.edu

Interaction between electron and photon is a fundamental research in physics. Such an interaction can be strongly enhanced by plasmon^{1 2 3}, which has an important role in many applications such as nanolasers^{4 5 6 7} and nanoantennas^{8 9 10 11}. Localized surface plasmons can be classified as bright modes and dark modes^{12 13 14}, which interact strongly and weakly with free photons, respectively. Here, we show that, dark plasmon in metal bowtie nanoantenna¹⁵ can strongly enhance the interaction between high energy electron and free photon, even though dark plasmon itself interacts weakly with free photons. Such a counterintuitive result is well-explained by our eigen-response theory^{12 13 16 17} as well as numerical simulations. Our experiment is also the most precise study of hybridization between localized plasmons to date.

Dark plasmon modes are weakly-radiative plasmon modes in nanostructures. Research interest in dark plasmon modes has been growing rapidly due to many potential applications^{12 13 14 18 19 20 21 22}. In particular, dark plasmon modes with high quality factors are important for making lasing devices in the nanoscale. Many novel dark-mode phenomena are also observed. For instance, it has been shown that the Fano resonances associated with the coupling between dark and bright modes can lead to extraordinary far-field phenomena^{19 20 22}. Recently, dark plasmon modes have been observed in optical nanoantennas using electronic excitation^{23 24 25}. So far, the interaction between photon and electron mediated by these dark plasmon modes is not yet studied experimentally.

Dark plasmon mode seems to be difficult to be measured by far-field optical techniques because of its weak radiation. In contrary, we demonstrate that, by controlling the location of electron beam, dark plasmon mode in optical nanoantennas can strongly mediate the interaction between the electron beam and photon, allowing us to have high spectral resolution far-field characterization of the dark plasmon mode using the cathodoluminescence (CL) technique²⁶. To understand this intriguing phenomena, we need an eigen-response theory^{12 13 16 17} of resonance that explains the ratio between excitation and response of a system.

Here, we briefly introduce the eigen-response theory. For a given excitation field, $\mathbf{E}_{exc}(\mathbf{r}, \omega)$, the general response polarization (dipole density), $\mathbf{P}(\mathbf{r}, \omega)$, can be written as a linear combination of the eigenmodes, $\mathbf{P}_j(\mathbf{r}, \omega)$, where j is a label of one eigenmode. In an abstract-vector form, it is written as $|P\rangle = \sum_j \alpha_{\text{eig},j} |P_j\rangle \langle P_j | E_{exc}\rangle$.

Here, $|P_j\rangle$ and λ_j ($\equiv \alpha_{\text{eig},j}^{-1}$) are, respectively, the j -th eigenmode and the j -th eigenvalue of an operator M which is defined by $M|P\rangle = |E_{\text{exc}}\rangle$ [the relation between the excitation field $\mathbf{E}_{\text{exc}}(\mathbf{r}, \omega)$ and the response $\mathbf{P}(\mathbf{r}, \omega)$]. Since $\alpha_{\text{eig},j}$ has a dimension of polarizability, it is called eigen-polarizability¹⁷ of the j -th eigenmode. The prediction from this eigen-response theory is explained as follows. If a system supports one dark mode, $|P_D\rangle$, and one bright mode, $|P_B\rangle$, the final interaction with the radiation field (photon) can be described by the overlap between a plane wave and the response field: $\langle k|P\rangle = \alpha_{\text{eig},B} \langle k|P_B\rangle \langle P_B|E_{\text{exc}}\rangle + \alpha_{\text{eig},D} \langle k|P_D\rangle \langle P_D|E_{\text{exc}}\rangle$, where $|k\rangle$ represents a plane wave in the direction of \mathbf{k} . In general $\langle k|P_D\rangle$ has a magnitude much smaller than $\langle k|P_B\rangle$. However, a dark mode with high quality factor should also have larger α_{eig} at resonance. As a result, the magnitude of $\alpha_{\text{eig},D} \langle k|P_D\rangle$ can be comparable with $\alpha_{\text{eig},B} \langle k|P_B\rangle$. In addition, a crucial factor that determines the ultimate radiation is the projection magnitudes $\langle P_B|E_{\text{exc}}\rangle$ and $\langle P_D|E_{\text{exc}}\rangle$. By choosing a zero projection to the bright mode (i.e., making $\langle P_B|E_{\text{exc}}\rangle = 0$), we can have strong photon radiation dominated by the dark mode, which indicates a dark-mode-mediated strong interaction between electron and photon.

Dark modes can be formed in a system of coupled dipole resonators due to the hybridization among dipole modes¹³, such as in bowtie nanoantenna¹⁵. The hybridization diagram for a bowtie nanoantenna formed by two equilateral Au triangles is shown in Fig. 1a for the dominant dipole modes in single triangles. The plasmon modes with anti-parallel dipoles are called dark modes while that with parallel dipoles are called bright modes^{24 25}. It should be noted that the horizontal

parallel and anti-parallel modes are well-separated while the vertical parallel and anti-parallel modes are almost degenerate in mode frequency, which is almost the same as that of a single nanotriangle. The magnitudes of the eigenpolarizabilities, α_{eig} , of a pair of Au bowtie nanoantenna are shown in Fig. 1b with their peaks indicating the resonant frequencies.

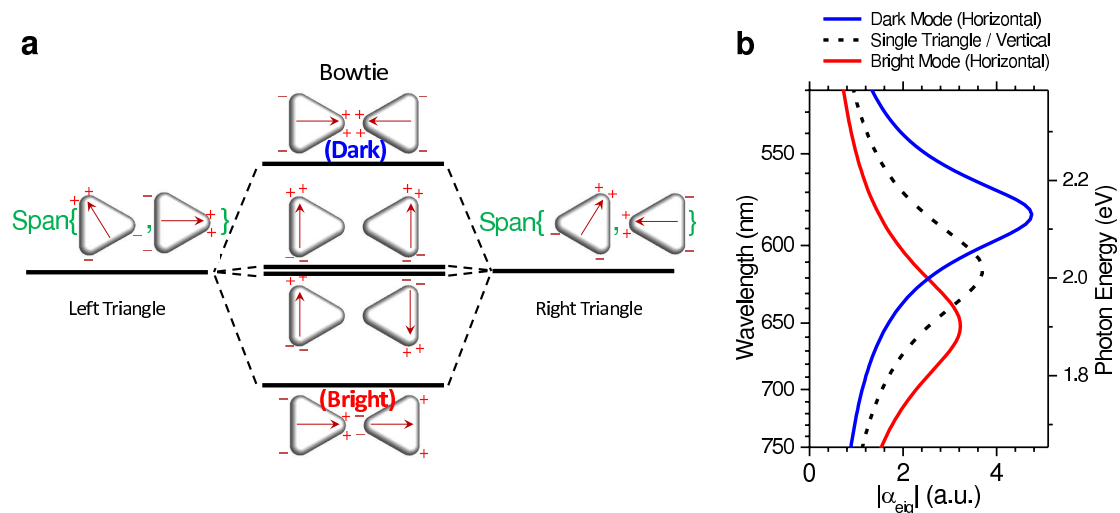


Figure 1 | Hybridization between the in-plane dipole plasmons of two equilateral triangles in tip-to-tip configuration (bowtie nanoantenna). **a**, Schematic diagram illustrating the hybridization between left and right particles. “Span” indicates the degenerate space spanned by the dipole modes. **b**, Magnitudes of the eigenpolarizabilities for the hybridized modes. The peaks indicate the resonant frequencies. Each Au particle has a tip-to-base size of 110 nm and thickness of 50 nm. Every corner/edge has a rounding radius of 15 nm.

In both of our simulation and experiment, a 30 keV electron beam is incident normally to a bowtie nanoantenna. Details of the experimental setup have been previously published^{27 28}. Sample preparation procedure is described in Methods. Simulation method is also described in Methods and the Supplementary Information in details. Fig. 2a shows a schematic of the problem considered. We simulate and

measure the photon emission for different fixed e-beam locations, which indicates the strength of the interaction between electron beam and photon.

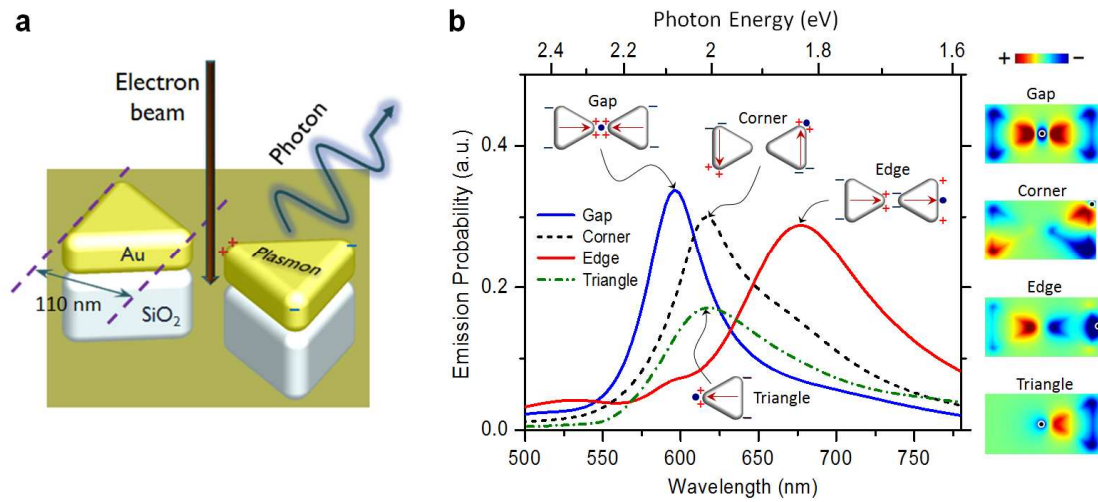


Figure. 2| CL spectra calculated by the FDTD method. a, The rounded bowtie structure used in numerical simulations. Each Au particle is lifted away from the substrate by a 85 nm thick SiO₂ layer of the same shape. **b,** Solid lines display the photon emission spectra for bowtie nanoantenna. Dashed line displays the spectrum for single triangle. The diagrams next to spectral peaks indicate the position of electron beams and the corresponding plasmon modes excited by the beam. Colored plots on the right show the field patterns on a plane that is 2 nm above the surface of the nanoantennas. The color indicates the electric field normal to the monitored plane, which can approximately represent the surface charge density.

Simulation results in Fig. 2b show that there is a dominant peak associated with each fixed e-beam. When the e-beam is fixed at the center (gap), right upper corner, and right edge of the bowtie antenna, we observe a peak at ~ 600 nm, 620 nm, and 680 nm, respectively. We see that there are at least three different plasmon modes supported by the bowtie antenna. This is consistent with our prediction that four resonant modes are supported while two of the modes are almost degenerate such that they can hardly be distinguished. To further verify our theory and understand the peaks, we also

simulate the case of single nanotriangle (dashed line in Fig. 2b). Such a peak wavelength corresponds to the dipole resonance of single nanotriangle while the peaks for gap, edge, and corner excitations correspond to anti-parallel horizontal dipoles, parallel horizontal dipoles, and vertical dipoles, respectively. The above classification of peaks is verified by simulating the field patterns at the corresponding peaks in Fig. 2b. The right colored panels in Fig. 2 show the z-component of the electric field at a plane located 2 nm above the surface of the bowtie nanoantenna for the three dominant peaks. These patterns can approximately represent the surface charge density. We see that, when fixing e-beam at the central gap and observing the field pattern at the wavelength of 600 nm, the distribution of the induced charges is symmetric in y-direction, which represents a pair of anti-parallel dipoles. For edge excitation at 680 nm, the induced charges show an almost antisymmetric distribution except the field produced by the e-beam itself near the right edge. For corner excitation at 620 nm, the induced charges show a pair of anti-parallel vertical dipoles. This agrees with our theory that the vertical modes have wavelengths very close to the single triangle case. Apart from the dominant peak positions, we also see some small features at shorter wavelengths, which may corresponds to higher order modes.

Here, we briefly discuss how different modes can be selectively excited. When we fix the e-beam at the center of the gap, the excitation field produced by the e-beam has an azimuthal symmetry with respect to the center of the bowtie. Therefore, only the plasmon with charge distribution symmetric in both directions can be excited ($\langle P_D | E_{exc} \rangle \neq 0$ and $\langle P_B | E_{exc} \rangle = 0$) and this leads to a pure excitation of horizontal anti-parallel dipole mode, which has the shortest wavelength among the three observable peaks. When the e-beam is fixed at the edge, a mirror symmetry is broken

and the excitation of the horizontal parallel dipole mode is possible ($\langle P_D | E_{exc} \rangle \neq 0$ and $\langle P_B | E_{exc} \rangle \neq 0$). Since the e-beam is far away from the center of bowtie nanoantenna, it is more favorable to the excitation of horizontal parallel mode, which leads to a peak at the longest wavelength. Similarly, in the case of e-beam fixed at the corner, the vertical dipole modes can be excited due to the broken mirror symmetry in the vertical direction. Details of the projection magnitudes and the emission strengths as a function of the position of electron beam are described in the Supplementary Information.

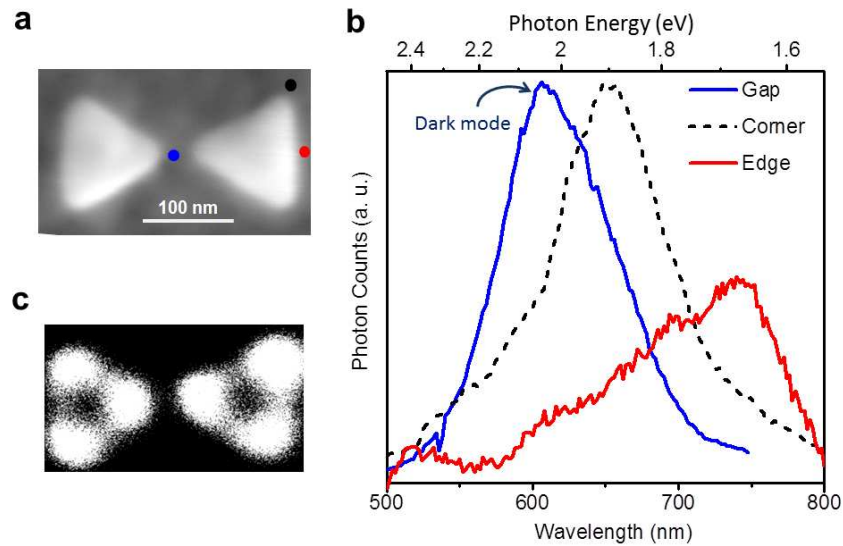


Figure 3| Experimentally measured CL spectra at different fixed beam locations. a, SEM picture of a fabricated bowtie antenna. **b,** Measured CL spectra at three locations indicated as colored dots in **c**. Panchromatic spatial image collected for the whole spectrum detected by the photodetector. Bright color corresponds to high photon counts.

Fig. 3 shows our experimental results. An SEM picture of the fabricated bowtie nanoantenna is shown in Fig. 3a. We observed three peaks for center (gap), corner, and edge excitations, indicated in the same SEM picture as blue, black, and red dots, respectively. The observation of the three modes is consistent with a previous related

experiment²⁵. The results (Fig. 3b) also agree well with the simulation results in terms of the number of peaks and relative peak positions, except the separation between peaks are larger in the experiment. The obtained peak wavelengths for center, corner, and edge excitations are, respectively, 600 nm, 650 nm, and 740 nm. We believe that the discrepancy from simulation results can be due to the detailed material and geometrical properties. The panchromatic CL image (Fig. 3c) also indicates that the edge excitation gives a weak signal even the bright mode is excited.

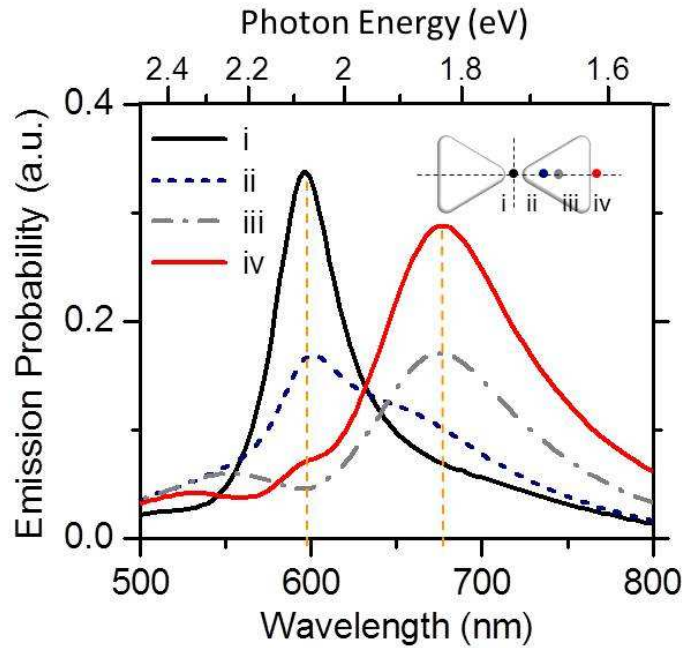


Figure. 4| Simulated CL spectra showing different projections of the excitation to parallel and anti-parallel modes. The locations of electron beam are shown in the inset. When the electron beam is fixed at i, only the horizontal anti-parallel dipole modes can be excited (i.e., $\langle P_B | E_{exc} \rangle = 0$), which leads to a single peak close to 600 nm. As we move the electron beam from i to iv, the horizontal parallel dipole modes (~ 680 nm) contribute more to the projection magnitude $\langle P_B | E_{exc} \rangle \neq 0$.

To further demonstrate the roles of projected magnitudes, we repeat the simulation by changing the position of the electron beam from the gap to the edge. The results in Fig. 4 show the effect of a gradual change in projection magnitude from domination of anti-parallel mode to parallel mode. We see there is no component of parallel mode contributing to the response when the e-beam is located at the gap and the radiation from the anti-parallel mode is thus the only dominant mode observed. It should be emphasized that the signal for position “i” is even higher than that of the parallel mode for position “iv”, indicating a strong interaction between electron beam and photon. This is also observed in our experimental results in Fig. 3b.

To conclude, we presented the first study of electron-photon interaction enhanced by dark plasmon modes. Our theory predicted that even though dark plasmon mode couples weakly with photon, it can strongly enhance the interaction between a high energy electron and photon. Our simulation and experiment strongly support the theoretical predictions. The result is beneficial to the development of experimental techniques for studying dark plasmon modes as well as the electron-photon interaction mediated by surface plasmons. The phenomenon presented in this letter is close to the classical limit. It would be interesting to study the quantum interaction in the future.

Methods

Simulation

Electron beam is modeled in FDTD simulation as a constantly moving point charge. After spatial discretization, the moving charge is approximated by a chain of pulsed source dipoles with time delays. Details of simulation method can be found in

Supplementary Information and elsewhere²⁷. The three dimensional geometry of the bowtie antenna in our simulation is almost the same as in the experiment, except the imperfection of the fabricated sample and the very thin (~3nm) adhesion layer below Au particles. To match the fabricated sample, all corner and edges in the model structure have a rounding radius of 15 nm.

Experiment

Bowtie antennas were fabricated using electron-beam lithography on a multilayered substrate with minimal background luminescence and relatively low substrate index²⁸. To avoid any background signal from native SiO₂²⁹, a 100 nm thick gold film was deposited onto a Si substrate using e-beam evaporation. 85 nm thick SiO₂ was deposited on top of this films using PECVD and 50 nm thick gold bowtie antennas were fabricated on this substrate using e-beam lithography. Subsequently, the oxide outside the antennas was removed using Freon based reactive-ion etching (RIE) in a CF₄ atmosphere leaving the antennas sitting on a very narrow oxide pillar. This approach allows minimal background noise as well as a low index substrate^{28 30}.

The samples were probed using a CL setup (Gatan MonoCL 3) incorporated into an SEM (JEOL 7000F). An Aluminum parabolic mirror, with a small hole for electron beam, placed on top of the sample collected the photons emitted by the antenna irradiated with an electron beam accelerated at 30 kV and 20 nA current. The collected photons were directed into a Mach-Czerny type monochromator to collect spectral information and imaging. For minimal damage the spectra were sampled at a rate of 0.5 sec per 2 nm while the images were taken at 0.5 msec per pixel (512x512 pixels). Control measurements were carried out on substrate gold film as well as gold-

oxide-gold sandwiched film that did not show any peaks except a weak 520 nm Au SPP peak as reported earlier²⁸.

Acknowledgments

This work was supported by National Science Foundation and the Office of Naval Research and carried out in part in the Frederick Seitz Materials Research Laboratory Central Facilities, University of Illinois, which are partially supported by the U.S. Department of Energy. We thank Dr. Jun Xu, Dr. Hyungjin Ma, Prof. C. T. Chan, and Prof. Lei Zhou for fruitful discussions.

Author contributions

K. H. F. and A. K. contributed equally to this study. A. K. carried out the sample fabrication and experiments. K. H. F. carried out the theoretical and numerical analysis. N. X. F. initiated and supervised the project. All authors discussed the results and commented on the manuscript at all stages.

References

¹ Ferrell, R. Predicted Radiation of Plasma Oscillations in Metal Films. *Phys. Rev.* **111**, 1214 (1958).

² Steinmann, W. Experimental verification of radiation of plasma oscillations in thin silver films. *Phys. Rev. Lett.* **5**, 470–472 (1960).

³ Brown, R. W., Wessel, P. & Trounson E. P. Plasmon reradiation from silver films *Phys. Rev. Lett.* **5**, 472–473 (1960).

⁴ Bergman, D. J. & Stockman, M. I. Surface plasmon amplification by stimulated

-
- emission of radiation: Quantum generation of coherent surface plasmons in nanosystems. *Phys. Rev. Lett.* **90**, 027402 (2003).
- ⁵ Hill, M T. *et al.* Lasing in metal-insulator-metal sub-wavelength plasmonic waveguides. *Opt. Express* **17**, 11107–11112 (2009).
- ⁶ Noginov, M. A. *et al.* Demonstration of a spaser-based nanolaser. *Nature* **460**, 1110–1113 (2009).
- ⁷ Oulton, R. F. *et al.* Plasmon lasers at deep subwavelength scale. *Nature* **461**, 629–632 (2009).
- ⁸ Mühlischlegel, P., Eisler, H.-J., Martin, O. J. F., Hecht, B. & Pohl, D. W. Resonant optical antennas. *Science* **308**, 1607 (2005).
- ⁹ Farahani, J. N., Pohl, D. W., Eisler, H.-J. & Hecht, B. Single Quantum Dot Coupled to a Scanning Optical Antenna: A Tunable Superemitter. *Phys. Rev. Lett.* **95**, 017402 (2005).
- ¹⁰ Taminiou, T. H., Stefani, F. D., Segerink, F. B. & van Hulst, N. F. Optical antennas direct single-molecule emission. *Nat. Photon.* **2**, 234–237 (2008).
- ¹¹ Pakizeh, T. & Käll, M. Unidirectional Ultracompact Optical Nanoantennas, *Nano Lett.* **9**, 2343–2349 (2009).
- ¹² Stockman, M. I., Faleev, S. V. & Bergman, D. J. Localization versus Delocalization of Surface Plasmons in Nanosystems: Can One State Have Both Characteristics? *Phys. Rev. Lett.* **87**, 167401 (2001).
- ¹³ Markel V. A. Antisymmetrical optical states. *J. Opt. Soc. Am. B* **12**, 1783–1791 (1995).
- ¹⁴ Benisty, H. Dark modes, slow modes, and coupling in multimode systems. *J. Opt. Soc. Am. B* **26**, 718–724 (2009).

-
- ¹⁵ Schuck, P. J., Fromm, D. P., Sundaramurthy, A., Kino, G. S. & Moerner, W. E. Improving the Mismatch between Light and Nanoscale Objects with Gold Bowtie Nanoantennas. *Phys. Rev. Lett.* **94**, 017402 (2005).
- ¹⁶ Bergman, D. J. & Stroud, D. Theory of resonances in the electromagnetic scattering by macroscopic bodies. *Phys. Rev. B* **22**, 3527–3539 (1980).
- ¹⁷ Fung, K. H. & Chan, C. T. Plasmonic modes in periodic metal nanoparticle chains: a direct dynamic eigenmode analysis. *Opt. Lett.* **32**, 973–975 (2007).
- ¹⁸ Giannini, V. *et al.* Controlling Light Localization and Light–Matter Interactions with Nanoplasmonics. *Small* **6**, 2498–2507 (2010).
- ¹⁹ Zhang, S., Genov, D. A., Wang, Y., Liu, M. & Zhang, X. Plasmon-Induced Transparency in Metamaterials. *Phys. Rev. Lett.* **101**, 047401 (2008).
- ²⁰ Liu, N. *et al.* Plasmonic analogue of electromagnetically induced transparency at the Drude damping limit. *Nat. Mater.* **8**, 758–762 (2009).
- ²¹ Lassiter, J. *et al.* Fano Resonances in Plasmonic Nanoclusters: Geometrical and Chemical Tunability. *Nano Lett.* **10**, 3184–3189 (2010).
- ²² Fan, Jonathan A. *et al.* Fano-like Interference in Self-Assembled Plasmonic Quadrumer Clusters. *Nano Lett.* **10**, 4680–4680 (2010).
- ²³ de Abajo, F. J. G. Optical excitations in electron microscopy. *Rev. Mod. Phys.* **82**, 209–275 (2010).
- ²⁴ Chu, M. W. *et al.* Probing Bright and Dark Surface-Plasmon Modes in Individual and Coupled Noble Metal Nanoparticles Using an Electron Beam. *Nano Lett.* **9**, 399–404 (2009).
- ²⁵ Koh, A. L., Fernández-Domínguez, A. I., McComb, D. W., Maier, S. A. & Yang, J. K. W. High-Resolution Mapping of Electron-Beam-Excited Plasmon Modes in Lithographically Defined Gold Nanostructures. *Nano Lett.* **11**, 1323–1330 (2011).

-
- ²⁶ Yacobi, B. G. & Holt, D. B. *Cathodoluminescence Microscopy of Inorganic Solids* (New York, Plenum, 1990).
- ²⁷ Chaturvedi, P. *et al.* Imaging of Plasmonic Modes of Silver Nanoparticles Using High-Resolution Cathodoluminescence Spectroscopy. *ACS Nano* **3**, 2965–2974 (2009).
- ²⁸ Kumar, A., Fung, K. H., Mabon, J. C., Chow, E. & Fang, N. X. Excitation and Imaging of Resonant Optical Modes of Au Triangular Nano-Antennas Using Cathodoluminescence Spectroscopy. *J. Vac. Sci. Technol. B* **28**, C6C21–C6C25 (2010).
- ²⁹ Liu, X., Phang, J. C. H., Chan, D. S. H. & Chim, W. K. The properties of 2.7 eV cathodoluminescence from SiO₂ film on Si substrate. *J. Phys. D: Appl. Phys.* **32**, 1563–1569 (1999).
- ³⁰ Hatab, N. A. *et al.* Free-Standing Optical Gold Bowtie Nanoantenna with Variable Gap Size for Enhanced Raman Spectroscopy. *Nano Lett.* **10**, 4952–4955 (2010).